

# Porosity Inducing Process Parameters in Selective Laser Melted AlSi10Mg Aluminium Alloy

R. Meneghello<sup>1</sup>, P. Ferro<sup>\*1</sup>, F. Berto<sup>2</sup>, S.M.J. Razavi<sup>2</sup>

<sup>a</sup> Department of Engineering and Management, University of Padova, Stradella San Nicola 3, 36100 Vicenza (Italy)

<sup>b</sup> NTNU, Department of Engineering Design and Materials, Richard Birkelands vei 2b, 7491, Trondheim (Norway)

\* Corresponding author: [paolo.ferro@unipd.it](mailto:paolo.ferro@unipd.it)

## Abstract

Additive Manufacturing techniques are known for the unrivalled geometric freedom they offer to designers. It's one of the mainstays of "metal 3D-printing", compared to casting, which, in contrast, implies more restrictions because some shapes won't cool down evenly or may need moulds or forms. Despite the possible presence of defects inside additive manufactured components, such as oxide films, pores or un-melted powder, they can be strongly reduced or controlled by process parameters optimization. That seems not true for a casting component, which defects could vary a lot from zone to zone according to the solidification conditions.

Porosity inducing process parameters in selective laser melted AlSi10Mg aluminium alloy are carefully analysed with the aim to find optimal conditions that guarantee the maximum material density and the best mechanical properties. Finally, a model is proposed that correlates the amount of pores with the alloy ultimate tensile strength.

Keywords: Additive manufacturing; Aluminium alloy; Selective Laser Melting, Porosity, Mechanical property

## 1. Introduction

Additive manufacturing (AM) first emerged in 1987 with stereolithography (SL) from 3D Systems, a process that solidifies thin layers of ultraviolet (UV) light-sensitive liquid polymer using a laser. Starting from that period, different AM processes developed so that, in 2010, the American Society for Testing and Materials (ASTM) group “ASTM F42 – Additive Manufacturing”, formulated a set of standards that classify the range of Additive Manufacturing processes into seven categories (Standard Terminology for Additive Manufacturing Technologies, 2012) [1]: VAT Photopolymerisation, Material Jetting, Binder Jetting, Material Extrusion, Powder Bed Fusion, Sheet Lamination, Directed Energy Deposition. Additive manufacturing offers several advantages throughout the design workflow including little lead time, few constraints, little-skill manufacturing. Furthermore, it is a low environmental impact process because it is characterized by less waste and energy saving. As a matter of fact, when compared with traditional manufacturing processes, additive manufacturing can significantly reduce energy usage by using less material and eliminating steps in the production process.

A significant problem with this type of production stands up in failure assessment. The material properties of AM components change depending on the fabrication process making it dependent on the geometry of the components. This means that every change in the geometry will change the way that the AM machine performs its fabrication routine affecting the properties of the resulting solid [2-4]. Currently, the main challenges for laser and metal powder-based AM include the formation of defects (e.g., porosity), low surface finish quality, and spatially non-uniform properties of the material. Such challenges stem largely from the limited knowledge of complex physical processes in AM especially the molten pool physics such as melting, molten metal flow, heat conduction, vaporization of alloying elements, and solidification.

Among the aluminium alloys, AlSi10Mg is certainly the most used for fabricating components through selective laser melting (SLM) process. Such alloy is often used in components of motor

racing, automotive industry, and general engineering. It has historically been a right choice for lightweight and thin-walled casting parts or any components with a complex geometry subjected to high loads. Generally, this aluminium alloy offers an economic alternative to titanium in the case of lightweight components exposed to non-critical fatigue and mechanical loads.

Today, AlSi10Mg is the most used aluminium alloy by laser melting techniques mostly because of its reduced susceptibility to cracking during solidification compared to others Al alloys (6xxx series in particular). However, the high thermal conductivity of aluminium and its alloys makes them notoriously difficult to cast and weld. For laser melting, things get even worse. Aluminium powders are highly reflective and have a high thermal conductivity when compared to other materials.

Therefore, high laser power is required to overcome the conductive cooling (rapid heat dissipation) into the surrounding material and melt the powder particles.

Another layer of complications comes from the susceptibility of these alloys to porosity formation mechanisms. In this regard, the sensibility of Al to surface oxidation and moisture pick-up are two major causes. Provided the powder was conditioned properly from the beginning and is still devoid of oxide films, this undesirable effect can be mitigated during the SLM process with strong fluxes of an inert atmosphere. However, since the formation of oxide films can't be avoided completely, the high laser power recommended to process aluminium alloys is required not solely to compensate heat diffusion, but also to disrupt oxide films.

AlSi10Mg parts issued from powder-bed additive layer manufacturing (ALM) processes exhibit higher or at least, comparable, mechanical properties than casted parts [5]. In particular, the ultimate tensile strength of the as-built Aluminium ALM parts is always higher than those obtained by High Pressure Die Casting (HPDC) in either as-casted or in the aged condition. While in the casting of AlSi10Mg parts, the hardness and strength increase during the heat treatment with the precipitation of intermetallic compounds ( $Mg_2Si$ ), in ALM parts, however, higher hardness and strength are already reached in the as-built state because of the very fine microstructure the rapid

cooling allows. Another contribution comes from the fine distribution of the Si phase in the Aluminium matrix as well as the presence of intermetallic compounds (i.e.  $Mg_2Si$ ).

Static and fatigue properties of additive manufactured AlSi10Mg samples obtained by SLM were investigated by Brandl et al. [6]. Mechanical properties were highly influenced by the building direction; however, the combination of 300 °C platform heating and peak-hardening were found to increase the fatigue and static resistance, neutralizing at the same time the building direction effect. Unfortunately, in that work, process parameters optimization was not taken into account.

With the objective to increase the process efficiency, in 2011 Buchbinder et al. [7], tried to increase the build rate of AM AlSi10Mg parts by using a 1 kW laser, while reaching a 99.5% material density. They demonstrated the possibility to extend the built rate from approximately 5 mm<sup>3</sup>/s to 21 mm<sup>3</sup>/s. In a recent paper, Han et al. [8] investigated the selective laser melting AlSi10Mg cellular lattice strut in terms of molten pool morphology, surface roughness, and dimensional accuracy. The results showed that the average width and depth of the molten pool, the lower surface roughness and dimensional deviation decrease with the increase of scanning speed and hatch spacing. In that work, the laser power was kept constant (200 W). The influence of laser power, scan speed, scan spacing and island size on porosity development in AlSi10Mg alloy builds has been investigated by Read et al. [9]. They found that the laser power, scan speed, and the interaction between the scan speed and scan spacing have a major influence on the porosity development in the builds. They also demonstrated the higher strength and elongation properties of SLMed samples compared to those of die-cast samples of similar composition.

Aboulkhair et al [10] investigated the effect of scanning speed (in the range of 250-1000 mm/s) and hatch spacing (from 50 to 250 μm) on porosity in AlSi10Mg parts processed by SLM. The laser power was kept constant and equal to 100 W. Surveying the windows of parameters, the best combination was found to be a speed of 500 mm/s and hatch spacing 50 μm when using a layer thickness of 40 μm and employing the pre-sinter scan strategy yielding a relative density of 99.8 %

In their work, Hasmuni et al. [11] focused their study in porosity inducing hatch distance in fabricated SLM AlSi10Mg parts. The hatch distance was varied from 0.1 to 0.15 mm while the laser power, the scanning speed, and the layer thickness were kept constant and equal to 350 W, 1650 mm/s and 30  $\mu\text{m}$ , respectively. The lowest porosity amount was obtained by using a hatch distance of 0.13 mm.

The several papers present in literature about SLM applied to AlSi10Mg alloy confirms, from one hand the high interest of academic and industrial world on this topic, and on the other the need to still deepen the strong and complex interaction between process parameters, microstructure and mechanical properties that characterises the process. This work is aimed to contribute to covering this gap by analysing the influence of laser power and exposure time on porosity amount in SLMed parts. Finally, an equation was proposed that correlates the ultimate tensile strength with porosity.

## **2. Materials and Methods**

The analysed material is the AlSi10Mg hypoeutectic alloy, mostly used for aluminium castings. Its chemical composition is collected in table 1. The little amount of Mg (0.3-0.5 wt%) allows the reinforcement by natural or artificial aging while its near eutectic composition (Fig 1) enhances its castability.

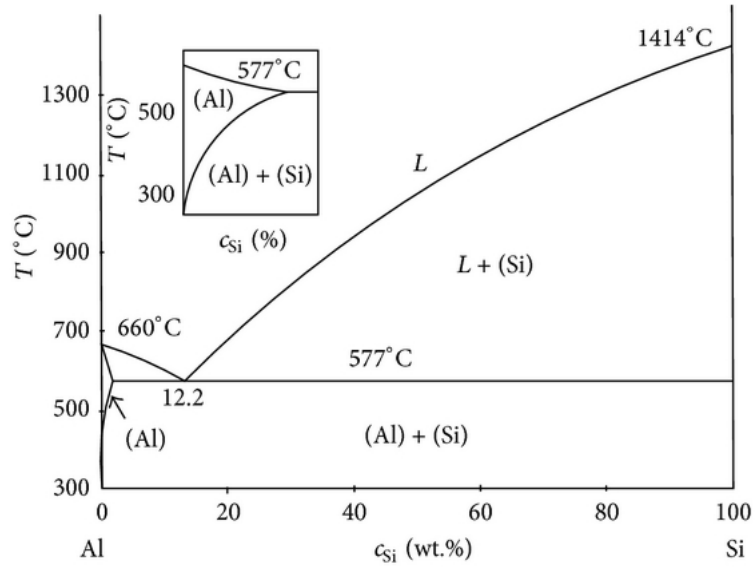


Fig. 1 –Aluminium-Silicon phase diagram

Al	Si	Mg	Fe	N	O	Ti	Zn	Mn	Ni	Cu	Pb	Sn
balance	9-11	0.25-0.45	<0.25	<0.2	<0.2	<0.15	<0.10	<0.10	<0.05	<0.05	<0.02	<0.02

Table 1 – Chemical composition of the alloy AlSi10Mg (wt%)

The particle size of the AlSi10Mg powder is in the range of 15-45  $\mu\text{m}$ .

The samples were obtained by selective laser melting with the 3d Printer Renishaw 400AM. The building square-based platform has a side length equal to 250 mm. The laser is characterized by 400 W maximum beam power with a diameter of 70  $\mu\text{m}$ . Argon was used as protective gas against powder oxidation. Both cylindrical (diameter and length equal to 10 mm) and dog bone specimens were produced following the Standard ASTM E606 (Fig. 2).

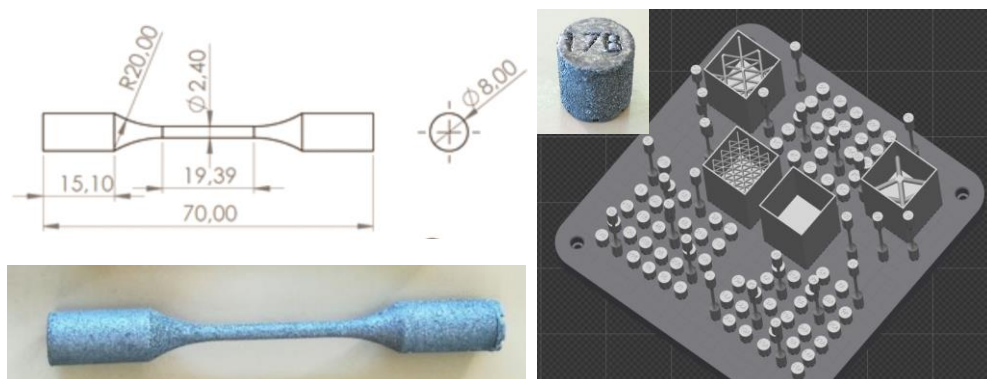


Fig. 2 - Geometry of the specimens (dimensions in mm) and their position on the building platform

In order to reduce the possible process parameters combinations, the following inputs were kept constant during the tests:

- Layer thickness ( $d$ ), 30  $\mu\text{m}$
- Spot diameter ( $\Phi$ ), 70  $\mu\text{m}$
- Platform temperature, 170  $^{\circ}\text{C}$
- Point distance ( $s$ ) equal to hatch distance ( $h$ ), 80  $\mu\text{m}$
- Building direction: sample axis

In Fig. 3 the laser scanning strategy and the definition of point distance and hatch distance are shown.

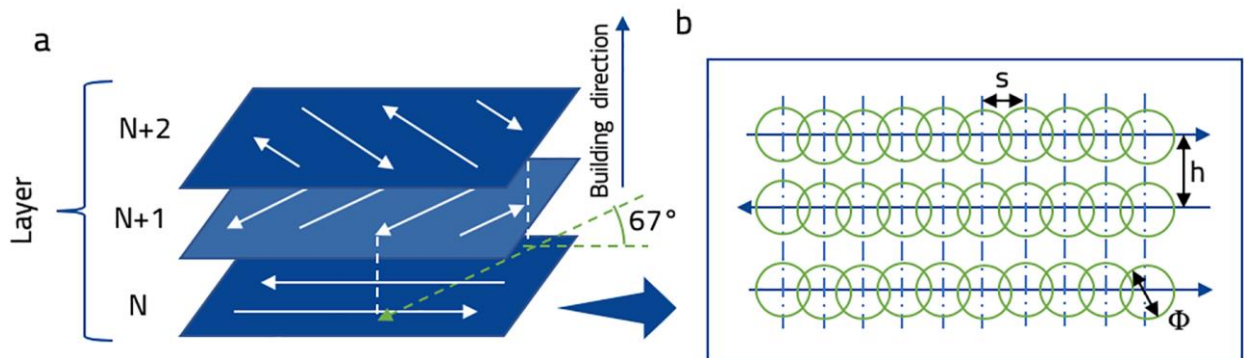


Fig. 3 – Scanning strategy (a); spot-to-spot fabrication process, where ‘s’ is the point distance, ‘ $\Phi$ ’ is the laser beam spot, and h is the hatch distance (b).

With the aim to minimize the porosity inside the material, the laser beam power and exposure time values were changed starting from those suggested by Renishaw (say, 275 W and 40  $\mu\text{s}$ ,

respectively). Three cylindrical samples for each couple of process parameters shown in Fig. 4 were carried out.

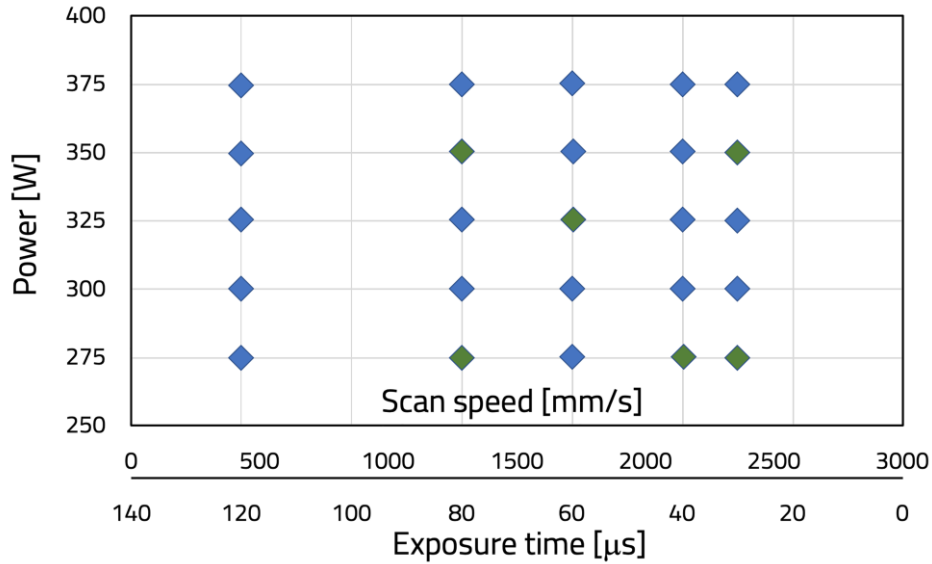


Fig. 4 – Process parameters tested in the experiment

In order to optimize the material at disposal, samples for tensile tests were produced with the couples of parameters marked in green in Fig. 4. It is noted that even if it was not possible to change the scan speed ( $v_s$ ), this last parameter can be approximated with the following relation:

$$v_s \approx \frac{s}{\text{exposure time}} \quad (1)$$

Samples for microstructural analyses were embedded in phenolic resin and prepared using standard grinding and polishing procedures. The microstructure was analysed using a scanning electron microscope (Quanta 2580 FEG, FEI, Boston, MA, USA). Light microscopy pictures were also taken with Leica DMC 2900 microscope. With the help of a dedicated software for image analysis, the microscope is driven to obtain the overall specimen image by means of the combinations of several micrographs carried out by scanning the entire surface of the specimen. The final micrograph is then processed for the automatic counting of the area interested by porosity. Fig. 5 shows the result of the micrographs processing routine above described for two cylindrical samples.

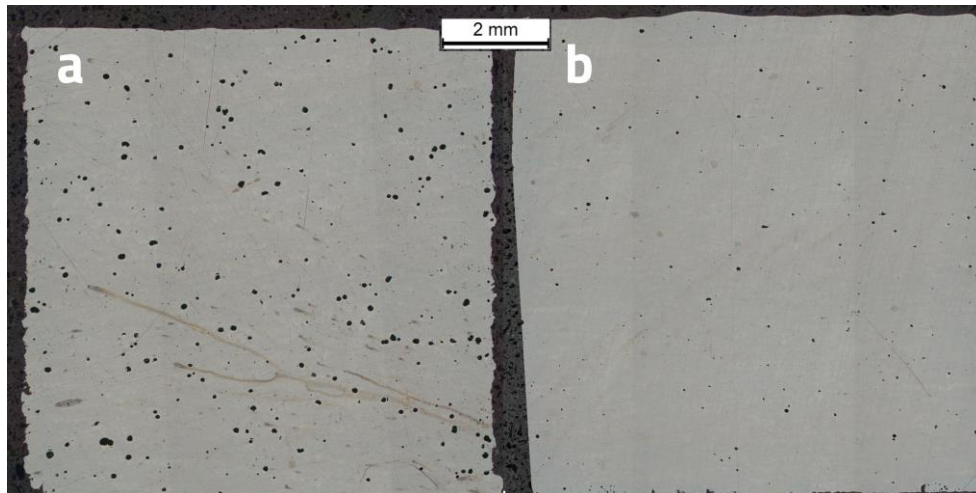


Fig. 5 – Processed image for the porosity amount assessment (samples obtained with: (a) power = 375 W, exposure time = 30  $\mu$ s; (b) power = 300 W, exposure time = 30  $\mu$ s)

The tensile tests were carried out by using the MTS Acumen 3 and following the Standard ISO 6892-1:2016. Fig. 6 shows the tensile specimen geometrical parameters. Samples obtained with the power and exposure time equal to 350 W and 80  $\mu$ s, respectively, were not tested because of their high deformation resulted after the building process.

### **3. Results and discussion**

#### *3.1 Microstructure*

Due to the incomplete homologous wetting and balling effects, pores are easily formed during the SLM process. Fig. 7 shows the pores morphology; gas porosity and sometimes balling were the most common defects observed. According to the phase diagram (Fig. 1) the microstructure (Fig. 7c) is characterized by  $\alpha$ -Al dendrites inside a eutectic matrix constituted by  $\alpha$ -Al and Si-particles.

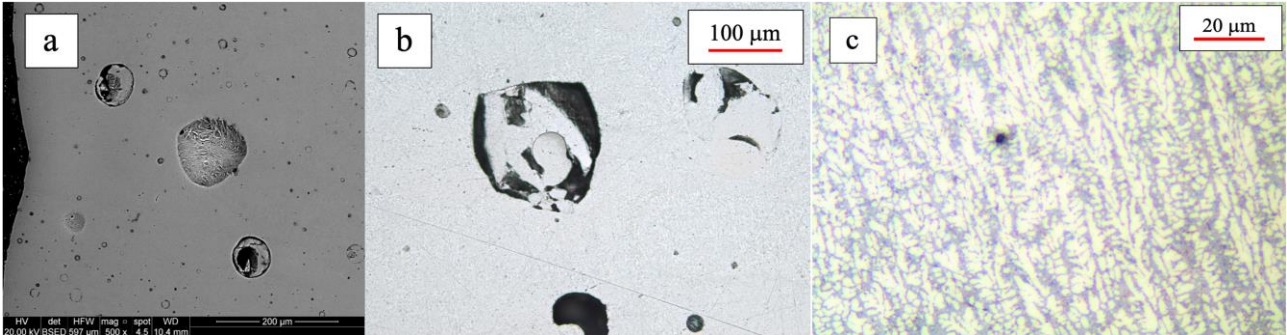


Fig. 7 – Pores morphology (a), ‘balling’ (b) and microstructure morphology (c) induced by SLM process (Power = 350 W; exposure time = 120 μs).

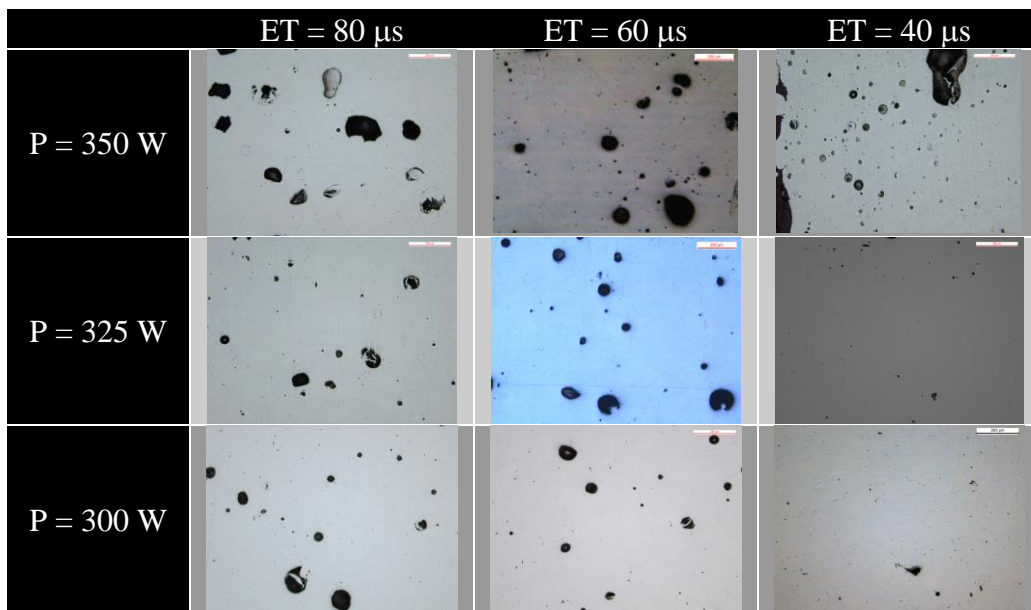


Fig. 8 - Some micrographs (magnifications 50x) showing porosity as a function of laser power (P) and exposure time (ET)

Fig. 8 shows some micrographs taken from cylindrical samples obtained by varying both the laser power (P) and the exposure time (ET). It is noted that samples containing lower amounts of pores are those obtained with the lower value of exposure time and laser power. For the sake of simplicity, Fig. 8 collects only the most significant micrographs as a function of a limited range of process parameters tested. On the other hand, the mean value of the area percentage occupied by pores as a function of the entire range of tested process parameters is shown in Fig. 9, where the bubble areas are proportional to the porosity percentage detected in the cylindrical samples.

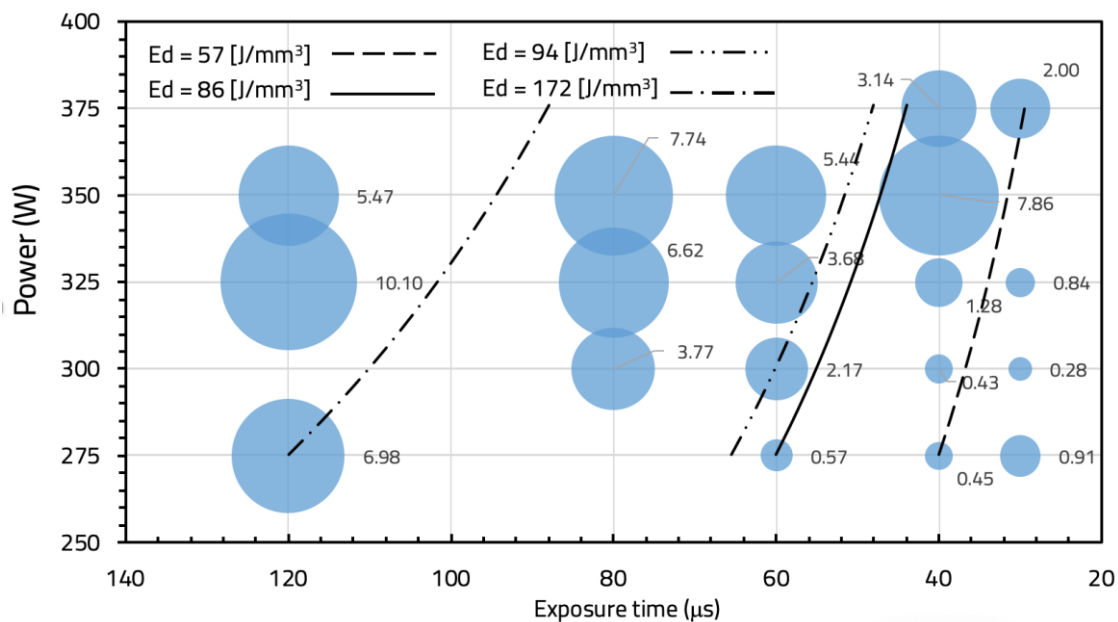


Fig. 9 – Porosity percentage (%) as a function of process parameters (laser power, exposure time) and energy density (Ed)

It is observed that minimum values of porosity are reached in the lower right corner of the graph (Fig. 9). Similarly, by using the concept of energy density (Ed), given by [11]:

$$Ed = \frac{P}{v_s \cdot h \cdot d} \quad (2)$$

it can be easily noted that samples characterized by the highest density, stay in the zone crossed by iso-energy density curves having the lowest values, in the range of tested parameters (Fig. 9).

Nevertheless, as observed by Prashanth et al. [12], the applicability of Eq. (2) is still at stake, even though it has been widely used in literature for optimizing the SLM parameters [11]. As a matter of fact, the Eq. (1) may not properly represent the effective energy transferred to melt the powder bed, and thus it needs to be improved involving the material properties. With the aim to reinforce that idea, the graph energy density versus porosity is plotted in Fig. 10. It shows the positive trend of porosity versus energy density but with a high scattering ( $R^2 = 0.6$ ). Despite this, results obtained are in agreement with those published by Read et al. [8] who found the minimum pores fraction induced by a critical energy density equal to approximately  $60 \text{ J/mm}^3$ . Finally, it's worth noting to observe that the equivalent mean pore diameter decreases as the energy density decreases (Fig. 11). Furthermore, the lower the energy density, the lower the standard deviation. To the best of the authors knowledge, this SLM feature has not been shown in previous work about this topic despite its advantage compared to casting components. Irrespective of the sample dimensions and thickness variations, the solidification defects induced by SLM process depend only by process parameters and do not vary from zone to zone of the component. On the contrary, solidification defects in casted parts strongly depend on both process parameters and casting dimensions. The higher the casting dimensions or thickness variations, the lower the microstructure homogeneity resulting from the corresponding different cooling conditions.

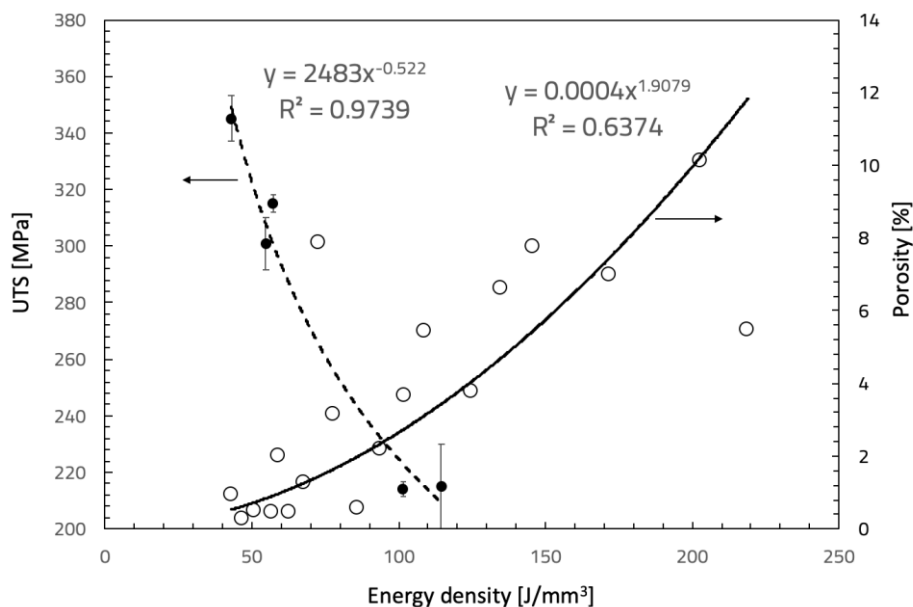


Fig. 10 - Porosity and UTS versus energy density

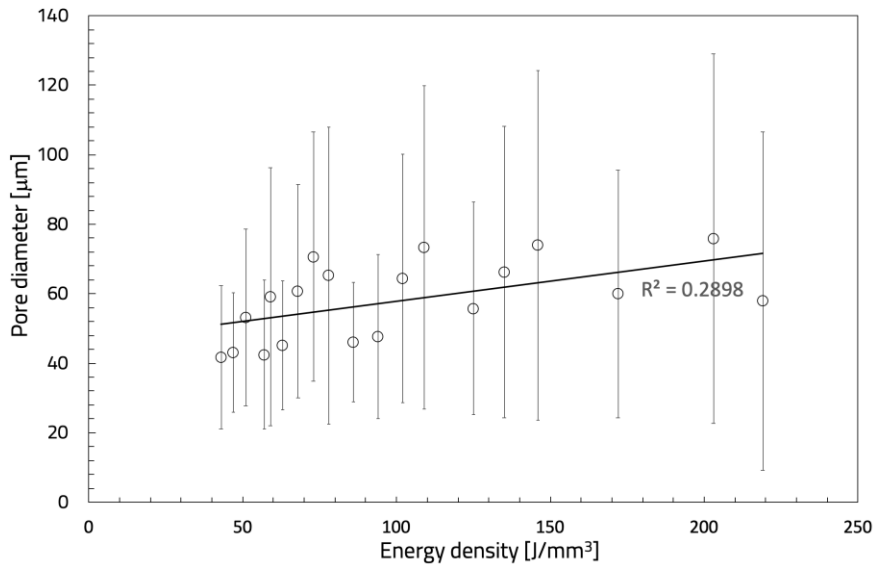


Fig. 11 – Equivalent mean pore diameter as a function of energy density.

### 3.2 Tensile tests

As expected, tensile strength is linked to the microstructure morphology, with particular reference to defects. The higher the porosity percentage, the lower the ultimate tensile strength (Fig. 10). A negative trend characterizes the UTS versus the energy density. This is attributed both to stress concentration effect and nominal cross-section area reduction induced by the porosity itself. Basing on this idea the following relation is proposed that correlates the UTS with the porosity ( $p$  [%]):

$$UTS = UTS_0 \left(1 - \frac{p}{100}\right)^n \quad (3)$$

where  $UTS_0$  is the ultimate tensile strength of the sample without porosity and  $n$  a material parameter, the values of which are obtained by the best fitting with experimental data. Fig. 11 shows the obtained result with  $UTS_0$  and  $n$  equal to 338 and 10, respectively.

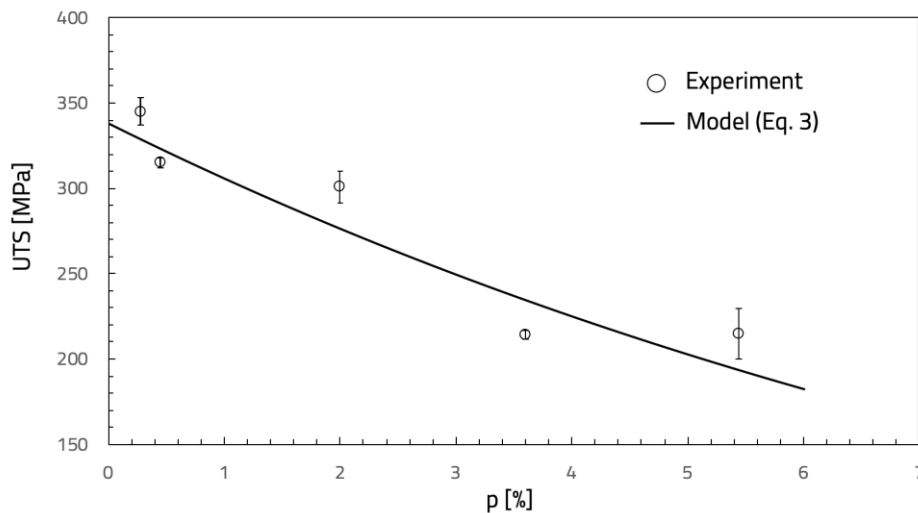


Fig. 11 – UTS versus porosity

#### 4. Conclusions

Porosity inducing process parameters in SLMed AlSi10Mg samples were studied. Because of the several parameters characterizing the process, layer thickness, spot diameter, platform temperature, point distance, hatch distance, and building direction were kept constant. The laser power and the exposure time have been varied from 275 W to 375 W and 30  $\mu$ s to 120  $\mu$ s, respectively. Tensile tests were finally carried out on samples produced with different process parameters. Results were described as a function of energy density and are summarized as follows:

- gas porosity is the main defect detected in the microstructure,

- the mean pore diameter value and its standard deviation decreases as the energy density decreases,
- minimum values of porosity percentage are obtained with the minimum values of energy density, between approximately 60 and 50 J/mm<sup>3</sup>,
- the higher the porosity percentage, the lower the UTS; an equation was finally proposed to model such behaviour.

## References

- [1] Standard Terminology for Additive Manufacturing Technologies: Designation F2792-12a. ASTM Committee F42 on Additive Manufacturing Technologies, ASTM Committee F42 on Additive Manufacturing Technologies. Subcommittee F42.91 on Terminology. *ASTM International*, 2012
- [2] S.M.J. Razavi, P. Ferro, F. Berto, J. Torgersen. Fatigue strength of blunt V-notched specimens produced by selective laser melting of Ti-6Al-4V. *Theoretical and Applied Fracture Mechanics*. vol. 13, 2018, 74-78
- [3] S.M.J. Razavi, P. Ferro, and F. Berto. Fatigue Assessment of Ti-6Al-4V Circular Notched Specimens Produced by Selective Laser Melting. *Metals*, 7, 2017, 291
- [4] S.M.J. Razavi, G. G. Bordonaro, P. Ferro, J. Torgersen and F. Berto. Fatigue Behavior of Porous Ti-6Al-4V Made by Laser-Engineered Net Shaping, *Materials* 11, 2018, 284
- [5] K. Kempena, L.Thijs, J. Van Humbeeck and J.-P. Kruth. Mechanical properties of AlSi10Mg produced by Selective Laser Melting. *Physics Procedia* 39 (2012) 439 – 446.
- [6] E. Brandl, U. Heckenberger, V. Holzinger, D. Buchbinder. Additive manufactured AlSi10Mg samples using Selective Laser Melting (SLM): Microstructure, high cycle fatigue, and fracture behaviour. *Materials and Design* 34 (2012) 159–169

- [7] Buchbinder, D, Schleifenbaum, H., Heidrich, S. , Meiners, W., Bültmann, J. High Power Selective Laser Melting (HP SLM) of Aluminum Parts. *Physics Procedia* 12 (2011) 271–278.
- [8] Xuesong Han, Haihong Zhu, Xiaojia Nie, Guoqing Wang and Xiaoyan Zeng. Investigation on Selective Laser Melting AlSi10Mg Cellular Lattice Strut: Molten Pool Morphology, Surface Roughness and Dimensional Accuracy. *Materials* 2018, 11(3), 392-405
- [9] Noriko Read, Wei Wang, Khamis Essa, Moataz M. Attallah. Selective laser melting of AlSi10Mg alloy: Process optimisation and mechanical properties development. *Materials & Design*, 65 (2015) 417- 424.
- [10] Nesma T. Aboulkhair, Nicola M. Everitt, Ian Ashcroft, Chris Tuck. Reducing porosity in AlSi10Mg parts processed by selective laser melting. *Additive Manufacturing*, 1–4 (2014) 77–86
- [11] Francesco Trevisan, Flaviana Calignano, Massimo Lorusso, Jukka Pakkanen, Alberta Aversa, Elisa Paola Ambrosio, Mariangela Lombardi, Paolo Fino and Diego Manfredi. On the Selective Laser Melting (SLM) of the AlSi10Mg Alloy: Process, Microstructure, and Mechanical Properties. *Materials* 10 (2017) 76-99
- [12] K. G. Prashanth, S. Scudino, T. Maity, J. Das & J. Eckert (2017) Is the energy density a reliable parameter for materials synthesis by selective laser melting? *Materials Research Letters*, 5:6, 386-390